AFRL-RX-WP-TP-2011-4385

GROWTH STRESS IN SiO2 DURING OXIDATION OF SiC FIBERS (PREPRINT)

Randall S. Hay

Ceramics Branch
Metals, Ceramics & Nondestructive Evaluation Division

NOVEMBER 2011

AIR FORCE RESEARCH LABORATORY
MATERIALS AND MANUFACTURING DIRECTORATE
WRIGHT-PATTERSON AIR FORCE BASE, OH 45433-7750
AIR FORCE MATERIEL COMMAND
UNITED STATES AIR FORCE

REPORT DOCUMENTATION PAGE

Form Approved
OMB No. 0704-0188

1. REPORT DATE *(DD-MM-YY)*	2. REPORT TYPE	3. DATES COVERED *(From - To)*
November 2011	Technical Paper	1 August 2011 – 1 August 2011

4. TITLE AND SUBTITLE
GROWTH STRESS IN SiO2 DURING OXIDATION OF SiC FIBERS (PREPRINT)

5a. CONTRACT NUMBER
In-house

5b. GRANT NUMBER

5c. PROGRAM ELEMENT NUMBER
62102F

6. AUTHOR(S)
Randall S. Hay

5d. PROJECT NUMBER
4347

5e. TASK NUMBER
50

5f. WORK UNIT NUMBER
LN102102

7. PERFORMING ORGANIZATION NAME(S) AND ADDRESS(ES)
Ceramics Branch/Metals, Ceramics & Nondestructive Evaluation Division
Air Force Research Laboratory, Materials and Manufacturing Directorate
Wright-Patterson Air Force Base, OH 45433-7750
Air Force Materiel Command, United States Air Force

8. PERFORMING ORGANIZATION REPORT NUMBER
AFRL-RX-WP-TP-2011-4385

9. SPONSORING/MONITORING AGENCY NAME(S) AND ADDRESS(ES)
Air Force Research Laboratory
Materials and Manufacturing Directorate
Wright-Patterson Air Force Base, OH 45433-7750
Air Force Materiel Command
United States Air Force

10. SPONSORING/MONITORING AGENCY ACRONYM(S)
AFRL/RXLN

11. SPONSORING/MONITORING AGENCY REPORT NUMBER(S)
AFRL-RX-WP-TP-2011-4385

12. DISTRIBUTION/AVAILABILITY STATEMENT
Approved for public release; distribution unlimited.

13. SUPPLEMENTARY NOTES
This is a work of the U.S. Government and is not subject to copyright protection in the United States. PA Case Number and clearance date: 88ABW-2011-4233, 3 Aug 2011. This document contains color.

14. ABSTRACT
A method to calculate the three principal growth stresses in SiO2 scales formed during SiC fiber oxidation has been developed. The method assumes that during oxidation the initial volume expansion at the SiC-SiO2 interface is three-dimensional and equal in all directions, and that subsequent SiO2 shear stress relaxation is described by the stress-dependent Eyring viscosity model. Large compressive stresses of ~10 GPa in SiO2 adjacent to the SiC-SiO2 interface are relaxed to much lower levels at all temperatures. At 1200° - 1300°C viscous flow of amorphous SiO2 further relaxes stress to negligible levels. At 700° - 900°C, axial and hoop stress at the GPa level persist. Radial stresses only reach values greater than 100 MPa at 700° - 900°C for scales thicker than ~0.1 fiber radii. Radial expansion of the scale eventually causes hoop stress and later axial stress to become tensile in the outer scale. Differences in stress-states developed for crystallized and uncrystallized scales are considered. Some tentative calculations for crystalline SiO2 scales are compared with experimental evidence for stress in the crystalline SiO2 scales of Hi-NicalonTM-S SiC fibers.

15. SUBJECT TERMS
SiC, residual stress, oxidation

16. SECURITY CLASSIFICATION OF:			17. LIMITATION OF ABSTRACT:	NUMBER OF PAGES	19a. NAME OF RESPONSIBLE PERSON (Monitor)
a. REPORT	b. ABSTRACT	c. THIS PAGE			Randall S. Hay
Unclassified	Unclassified	Unclassified	SAR	22	19b. TELEPHONE NUMBER *(Include Area Code)* N/A

Growth Stress in SiO_2 during Oxidation of SiC Fibers

R. S. Hay, Air Force Research Laboratory, WPAFB, OH

Abstract

A method to calculate the three principal growth stresses in SiO_2 scales formed during SiC fiber oxidation has been developed. The method assumes that during oxidation the initial volume expansion at the SiC-SiO_2 interface is three-dimensional and equal in all directions, and that subsequent SiO_2 shear stress relaxation is described by the stress-dependent Eyring viscosity model. Large compressive stresses of ~10 GPa in SiO_2 adjacent to the SiC-SiO_2 interface are relaxed to much lower levels at all temperatures. At 1200° - 1300°C viscous flow of amorphous SiO_2 further relaxes stress to negligible levels. At 700° - 900°C, axial and hoop stress at the GPa level persist. Radial stresses only reach values greater than 100 MPa at 700° - 900°C for scales thicker than ~0.1 fiber radii. Radial expansion of the scale eventually causes hoop stress and later axial stress to become tensile in the outer scale. Differences in stress-states developed for crystallized and uncrystallized scales are considered. Some tentative calculations for crystalline SiO_2 scales are compared with experimental evidence for stress in the crystalline SiO_2 scales of Hi-Nicalon™-S SiC fibers. Assumptions and limitations of the method are discussed, along with implications for fiber strength and oxidation kinetics.

I. Introduction

Passive oxidation of SiC to SiO_2 is in most cases controlled by interstitial diffusion of O_2 molecules through the amorphous or crystalline silica scale.[1-2] There is a volume expansion of ~2.2× during SiC oxidation to SiO_2. Constraint of this expansion at the SiC-SiO_2 interface generates very large stresses. Microstructural evidence for these stresses exists for crystalline scales. Cracks formed in crystalline scales during SiC fiber oxidation were attributed to tensile hoop growth stress in the outer scale.[3-5] These cracks function as short-circuit diffusion pathways for oxidation and render the scale non-passivating.[5-6] Tensile stress in the scale may also contribute to lower strengths during oxidation at high temperature.[7] Very high dislocation densities in crystalline SiO_2 near the SiC-SiO_2 interface scales suggests that very high shear stresses exist during scale growth near that interface.[5]

Oxidation of silicon to SiO_2 has a volume expansion similar to that for SiC oxidation. Large effort has been devoted to modeling growth stress during silicon oxidation at 700° - 1200°C.[8] These studies are motivated by the use of SiO_2 as a dielectric and a device isolation material in integrated circuits.[9-10] Numerical models using finite element or finite difference methods that are adaptable to a variety of silicon substrate geometries in integrated circuits have been developed to model oxidation growth stress.[8-9, 11-19] Analytical models for flat-plate and cylindrical silicon substrates have also been developed that predict differences in the growth stresses for the two geometries. Radial and axial compressive growth stress and tensile hoop growth stress are predicted for oxidation of silicon fibers.[20-22] For the flat plate geometry, only in-plane compressive growth stress is present.

The role of growth stress on oxidation mechanisms in silicon has been extensively analyzed and discussed.[23] Compressive growth stress reduces O_2 diffusivity in SiO_2,[8, 12, 20, 24-25] reducing Si oxidation rates.[26-28] Externally applied compressive stress has also been shown to decrease the rate of silicon oxidation.[29] Externally applied tensile stress increases those oxidation rates,[29-31] and recently the same has been demonstrated for SiC fibers.[32] However, growth stress modeling and analysis for SiC oxidation is lacking. Extensive characterization and analysis of carbon and SiOC layer formation at the SiC-SiO_2 interface during SiC oxidation has not considered the effects of growth stress.[2] Growth stress also contributes to the residual stress in SiO_2 scales on SiC fibers, which in turn may affect the crystallization rates of the scales and the strengths of oxidized fibers.[5]

Existing growth stress models for cylindrical silicon substrates assume that the volume expansion accompanying oxidation is either dilational (equal expansion in all directions),[7] uniaxial (all expansion in the radial direction),[7, 33-34] or nearly uniaxial but with a small intrinsic axial and hoop strain in the SiO_2 oxidation product.[20, 25] Most models assume stress is two-dimensional and ignore the axial stress (σ_z).[21, 25, 33-34] However, silicon wafer bending during oxidation can only be explained by three-dimensional expansion during oxidation.[8, 10] Early cylinder oxidation models assumed Newtonian viscous flow.[7, 21, 33] Most later models recognize that flow at high stress is non-Newtonian and use the Eyring model for stress-dependent viscosity.[20, 25, 34] Uniaxial expansion models with Newtonian flow predict high tensile hoop stress (σ_θ) at the SiC-SiO_2 interface that decreases towards the SiO_2 surface.[7, 21, 33] Models with stress-dependent viscosity predict compressive σ_θ at the SiC-SiO_2 interface that rapidly

changes to tension towards the SiO_2 surface.[20, 34] One model with stress-dependent viscosity considers only shear stress and does not attempt to resolve it into principal stresses.[25] No models calculate both σ_z and σ_θ for cylindrical substrates, or consider how the change in σ_θ from compressive to tensile affects shear stress, and how the relaxation of shear stress then separately affects σ_θ and σ_z . For structural SiC fibers this is an important omission because the σ_z component of residual stress that may affect fiber strength.

A method for computation of all three principal growth stresses throughout the thickness of an SiO_2 scale during oxidation of SiC fibers is presented. The method can be equally well applied to silicon fibers or cylinders. The model assumes oxidation volume expansion is three-dimensional (dilatational) and that the stresses resulting from constraint of that expansion are relaxed with an Eyring stress-dependent SiO_2 viscosity.[35] Growth stress calculations for oxidation of SiC fibers are done from 700° to 1300°C for amorphous scale thicknesses up to 3 μm. Some calculations are also done for crystalline scales using the very limited data available for cristobalite viscosity.[36-38] These calculations are compared with microstructural evidence for stress in crystalline scales on Hi-Nicalon™-S SiC fibers that has been previously published.[5] Possible effects of self stress on O_2 diffusion are discussed. The change in oxidation growth stress with fiber radii from 3 μm to → ~∞ (flat plate) are examined. Assumptions and limitations of the model are discussed.

II. Method

A. General

A schematic illustrating the volume expansion and the stresses associated with oxidation, as well as the discretization of SiC oxidation into annular SiO_2 layers is shown in figure 1. There are two sources of stress. The first is the 2.2× volume expansion from oxidation of SiC to SiO_2. This expansion is shown in stress-free and constrained states in figure 1. Constraint of that expansion by the underlying SiC and overlying SiO_2 causes extremely large axial (σ_z) and hoop (σ_θ) stress, and much smaller radial (σ_r) stress because $\sigma_r = 0$ at the scale surface and small scale thicknesses relative to fiber radii are usually of interest. σ_r increases or decreases through the scale thickness, depending on the sign and magnitude of σ_z and σ_θ. The stresses involved in constraint of the initial volume expansion are far larger than those for which linear elasticity theory is valid.[8] However, as pointed out previously,[25] even at low temperatures σ_z and σ_θ relax very rapidly from high levels by radial expansion to values appropriate for linear elasticity if the Eyring model for the dependence of viscosity on shear stress is used. The second source of stress is the circumferential expansion of old scale as it is radially displaced by the formation of new scale (Fig. 1). This creates tensile σ_θ in the older scale and eventually tensile σ_z by the Poisson effect.

A flowchart with the major calculation steps is shown in figure 2. A detailed description of the calculation methods in each step follows.

B. SiC Fiber Oxidation Kinetics

Fiber oxidation kinetics do not deviate significantly from those for flat plate geometry until the oxidation products for 12 μm diameter fibers are several microns thick,[5, 39] so SiO_2 thickness [$\mathbf{w(t)}$] (Fig. 1) is assumed to obey Deal-Grove kinetics for flat plate geometry:[5, 40]

$$w(t) = \frac{1}{2}A\sqrt{1 + \frac{4B(t + t_i)}{A^2}} - 1 \qquad [1a]$$

$$t_i = \frac{x_i^2 + Ax_i}{B} \qquad [1b]$$

where $\mathbf{t_i}$ is a time shift that corrects for the presence of an initial oxide layer $\mathbf{x_i}$, **B** is the parabolic rate constant and **B**/**A** is the linear rate constant. All growth stress modeling for amorphous SiO_2 assumes that $\mathbf{x_i}$=0, but for crystalline scales it is useful to consider the thickness at which the scale crystallizes as a stress-free state with thickness $\mathbf{x_i}$. **B** and **A** obey the usual Arrhenius relationships:

$$A = A_0 e^{\frac{-Q_A}{RT}} \qquad [2]$$

$$B = B_0 e^{\frac{-Q_B}{RT}} \quad [3]$$

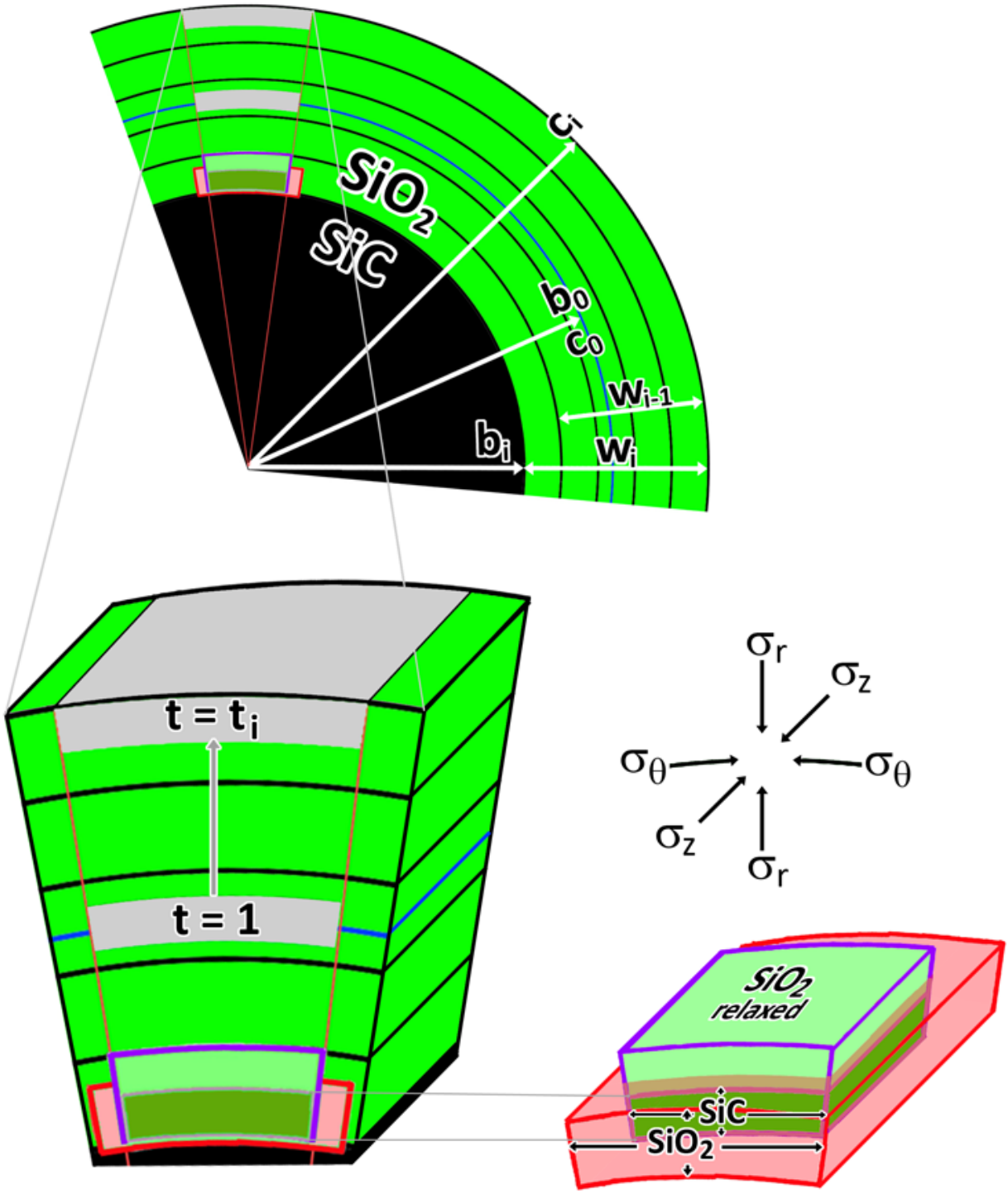

Fig. 1 Schematic diagrams of oxidation of SiC to SiO_2. Discretization of annular layers is illustrated and notated. Volume expansions and stresses associated with oxidation are indicated. The circumferential expansion of an old scale layer as it is pushed outward is also shown. The original SiC surface is shown as a blue line, roughly midway through the scale thickness. Original SiC is dark green, the elastically constrained SiO_2 oxidation product is light red, and the relaxed SiO_2 is light green with a purple boundary.

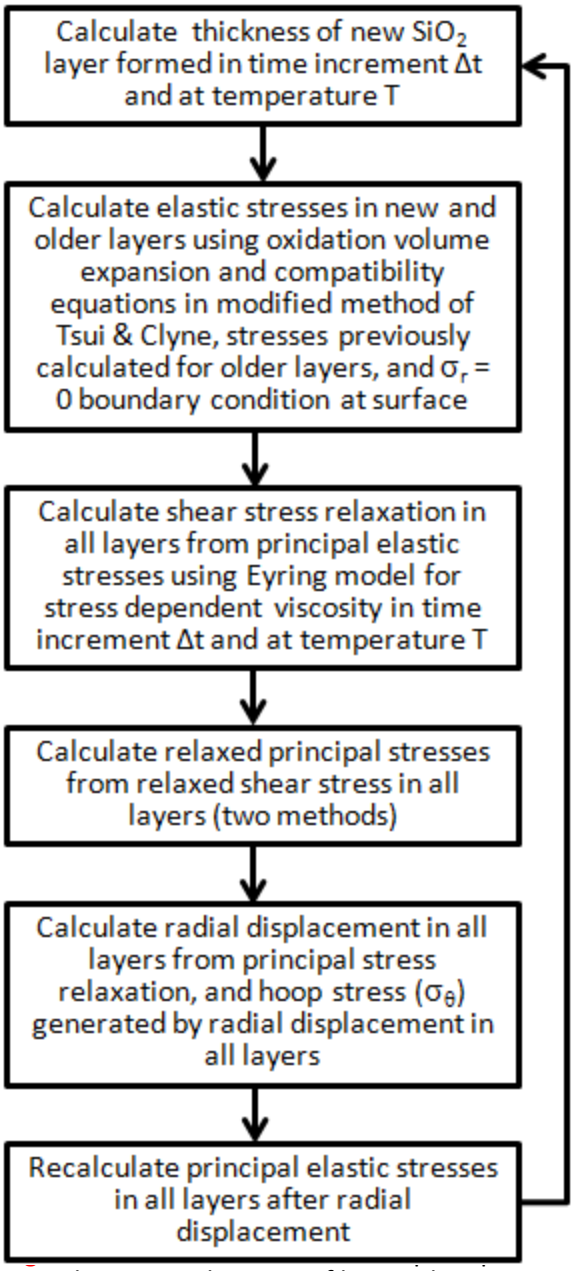

growth stresses during SiC fiber oxidation.

where **T** is absolute temperature, **R** is the gas constant, Q_A and Q_B are activation energies and A_o and B_o are pre-exponential factors. Recent work finds that $A_o = 4.7 \times 10^{-4}$ m, $Q_A = 110$ kJ/mol, $B_o = 1.2 \times 10^{-8}$ m^2/s, $Q_B = 248$ kJ/mol for Hi-Nicalon™-S SiC fiber oxidation.[5] The SiO_2 oxidation product has 2.2 × the volume of the SiC consumed. The SiC radius [**b**(**t**)] after oxidation for time t is (Fig. 1):

$$b(t) = \sqrt{w^2(\Omega^2 - \Omega) + b_o^2} - \Omega w \qquad [4]$$

where b_o is the original fiber radius (6.1 μm for Hi-Nicalon™-S)[5] and **Ω** is the ratio of SiC molar volume (Ω_{SiC}) to SiO_2 molar volume (Ω_{SiO_2}), sometimes referred to as the Pilling-Bedworth ratio:[33]

$$\Omega = \frac{\Omega_{SiC}}{\Omega_{SiO_2}} = \frac{12.46\ cm^3}{27.34\ cm^3} = 0.456 \qquad [5]$$

The outer radius of the SiO_2 scale [**c**(**t**)] is (Fig. 1):

$$c(t)=b(t)+w(t) \qquad [6]$$

C. *Elastic Growth Stress*

The elastic stresses and strains can be determined from a modification of a method used for progressively deposited coatings on cylinders.[41] This method was developed for sequentially deposited coatings, where the last coating is at the surface. During fiber oxidation the "deposition" sequence is reversed; the last oxide increment forms at the SiC-SiO_2 interface. The SiO_2 scale is therefore discretized into annular increments, or layers, formed in equal units of time, with the oldest layer at the surface.

The unrelaxed elastic growth stresses are calculated by dividing the SiC-SiO_2 system into three separate volumes – the unoxidized SiC fiber, the annular SiO_2 added from time **t**(i -1) to **t**(i) at the SiC-SiO_2 interface, and the outer (older) SiO_2 ring that was added from time **t**(0) to **t**(i-1) (Fig. 1). The axial, radial, and hoop stresses in the SiC fiber at time **t**(i) are designated $\sigma_z^{SiC}(i)$, $\sigma_r^{SiC}(i)$, and $\sigma_\theta^{SiC}(i)$ respectively. The axial, radial, and hoop stresses in the two annular SiO_2 layers are $\sigma_z^{SiO2}(i)$, $\sigma_r^{SiO2}(i)$, $\sigma_\theta^{SiO2}(i)$ and $\sigma_z^{SiO2}(i-1)$, $\sigma_r^{SiO2}(i-1)$, $\sigma_\theta^{SiO2}(i-1)$, respectively. The increment in SiO_2 thickness formed from time **t**=i-1 to **t**=i is therefore **w**(i)-**w**(i-1). The effect of adding the i^{th} SiO_2 layer on the principal stresses in the three separate volumes can be found from three equations for **f**, p_j, and p_{is}, using a modification of the method of Tsui and Clyne that uses strain compatibility equations:[41]

$$E_{SiO_2}\Delta\varepsilon = \sigma_z^{SiO_2}(i-1) - \sigma_z^{SiO_2}(i) + \upsilon_{SiO_2}\left(\sigma_\theta^{SiO_2}(i) - \sigma_\theta^{SiO_2}(i-1) + \sigma_r^{SiO_2}(i) - \sigma_r^{SiO_2}(i-1)\right) \qquad [7]$$

$$E_{SiO_2}\Delta\varepsilon = \sigma_\Theta^{SiO_2}(i-1) - \sigma_\theta^{SiO_2}(i) + \upsilon_{SiO_2}\left(\sigma_z^{SiO_2}(i) - \sigma_z^{SiO_2}(i-1) + \sigma_r^{SiO_2}(i) - \sigma_r^{SiO_2}(i-1)\right) \qquad [8]$$

$$\frac{1}{E_{SiO_2}}\left[\sigma_\theta^{SiO_2}(i) - \upsilon_{SiO_2}\left(\sigma_z^{SiO_2}(i) + \sigma_r^{SiO_2}(i)\right)\right] = \frac{1}{E_{SiC}}\left[\sigma_\theta^{SiC}(i) - \upsilon_{SiC}\left(\sigma_z^{SiC}(i) + \sigma_r^{SiC}(i)\right)\right] \quad [9]$$

where:

$$\Delta\varepsilon = \sqrt[3]{\frac{\Omega_{SiO_2}}{\Omega_{SiC}}} - 1 \quad [10]$$

$$\sigma_z^{SiC}(i) = \frac{-E_{SiC}f}{\pi\left(E_{SiC}b^2(i) + E_{SiO_2}\left(\left(b(i) + w(i) - w(i-1)\right)^2 - b^2(i)\right)\right)} + \sigma_z^{SiC}(i-1) \quad [11]$$

$$\sigma_r^{SiC}(i) = \sigma_r^{SiC}(i-1) - p_{is} \quad [12]$$

$$\sigma_\theta^{SiC}(i) = \sigma_\theta^{SiC}(i-1) - p_{is} \quad [13]$$

$$\sigma_z^{SiO_2}(i) = \frac{-E_{SiO_2}f}{\pi\left(E_{SiC}b(i)^2 + E_{SiO_2}\left(\left(b(i) + w(i)\right)^2 - b(i)^2\right)\right)} \quad [14]$$

$$\sigma_r^{SiO_2}(i) = -p_i \quad [15]$$

$$\sigma_\theta^{SiO_2}(i) = \frac{p_j\left(b(i) + w(i)\right)}{w(i) - w(i-1)} \quad [16]$$

$$\sigma_z^{SiO_2}(i-1) = \frac{f}{\pi\left[\left(b(i-1) + w(i-1) - w(i)\right)^2 - b^2(i-1)\right]} \quad [17]$$

$$\sigma_r^{SiO_2}(i-1) = 0 \quad [18]$$

$$\sigma_\theta^{SiO_2}(i-1) = \frac{2p_{is}b(i-1)^2 - p_i\left(\left(b(i-1) + w(i-1)\right)^2 + b(i-1)^2\right)}{\left(b(i-1) + w(i-1)\right)^2 - b(i-1)^2} \quad [19]$$

where **f** is the axial force, $\mathbf{p_{is}}$ is the pressure across the SiO_2-SiC interface, $\mathbf{p_i}$ is the pressure across the interface between the i^{th} and the $i\text{-}1^{th}$ SiO_2 layers, $\mathbf{E_{SiC}}$ and $\mathbf{E_{SiO2}}$ and Young's modulus of the SiC fiber and the SiO_2 scale, respectively, and $\boldsymbol{\nu_{SiC}}$ and $\boldsymbol{\nu_{SiO2}}$ are Poison's ratio for the SiC fiber and the SiO_2 scale.

Stresses in older layers (j = i-2 to j = 0) are updated with the i-1 stress values in [17 - 19]:

$$\sigma_z^{SiO_2}(j) = \sigma_z^{SiO_2}(j) + \sigma_z^{SiO_2}(i-1) \quad [20]$$

$$\sigma_r^{SiO_2}(j) = \sigma_r^{SiO_2}(j) + \sigma_r^{SiO_2}(i-1) \quad [21]$$

$$\sigma_\theta^{SiO_2}(j) = \sigma_\theta^{SiO_2}(j) + \sigma_\theta^{SiO_2}(i-1) \quad [22]$$

D. Relaxation of Shear Stress

The relaxation of the elastic stresses for all annular elements (j=1 to i) in time increment **Δt**=**t**(i)-t(i-1) are calculated next. Stress relaxation in the SiC substrate is assumed to be negligible. Deviation

from Newtonian viscosity, referred to as glass plasticity, results in lower effective viscosity at high shear stress. The Eyring model for shear stress ($\boldsymbol{\tau}$) dependence of glass viscosity ($\boldsymbol{\eta}$) is frequently used for viscosity:[8-9, 11-12, 14, 16, 18-20, 22, 25, 35, 42]

$$\eta = \eta_o \frac{\tau V_c/2kT}{\mathrm{Sinh}\left(\tau V_c/2kT\right)} = \eta_o \frac{\tau/\tau_c}{\mathrm{Sinh}\left(\tau/\tau_c\right)} \quad [23]$$

where the activation volume for plasticity in SiO_2, $\mathbf{V_c}$, decreases with temperature, and has been inferred to have values ranging between 1.2 ×10^{-28} m^3 to 3 × 10^{-28} m^3.[12, 20, 25] The parameter **k** is Boltzmann's constant, $\boldsymbol{\tau_c}$ is the critical shear stress above which plasticity is significant (typically ~ 150 MPa), and $\boldsymbol{\eta_o}$ is the stress-fee viscosity described by:[43-44]

$$\eta_o = C_o\, e^{\frac{Q}{RT}},\ C_0 = 3.8 \times 10^{-13}\ \&\ Q = 712{,}000\ \mathrm{kJ/mol} \quad [24]$$

from 1000°C to 1400°C. Unfortunately this relationship lacks experimental validation below 1000°C.[43-44] For silica formed from SiC oxidation, carbon in the SiO_2 scale may cause viscosities to be higher than those in [24].[45] The plasticity activation volume $\mathbf{V_c}$ corresponds to a critical shear stress $\boldsymbol{\tau_c}$ of about 100 MPa, which is roughly consistent with experiment at 500 to 1400°C.[42, 46] Shear stress relaxation with time obeys a Maxwell viscoelastic model:[12, 25, 47]

$$\frac{d\tau(t)}{dt} = -G\,\tau(t)/\eta(\tau)\ , \qquad \tau[t(i-1)] = \tau_o\, t(i-1) \quad [25]$$

where **G** is the SiO_2 shear modulus and the shear stress at the initial time t(i-1) is $\boldsymbol{\tau_o}$. The shear modulus (**G**) of amorphous silica is 34 GPa, with only weak temperature dependence.[48] The relaxation of shear stress with time (τ(t)) can be determined by substitution of [23-24] in [25] and solving the resulting differential equation [25] for $\boldsymbol{\tau}$[t]:

$$\tau[t] = \frac{4kT}{V_c}\mathrm{Coth}^{-1}\left[\frac{e^{\frac{Gt}{\eta_o}}}{\sqrt{\mathrm{Tanh}\left[\frac{V_c\tau_o}{4kT}\right]^2}}\right] = 2\tau_c\mathrm{Coth}^{-1}\left[\frac{e^{\frac{Gt}{\eta_o}}}{\sqrt{\mathrm{Tanh}\left[\frac{\tau_o}{2\tau_c}\right]^2}}\right] \quad [26]$$

The initial shear stress $\boldsymbol{\tau_o}$ is determined from the principal stresses for all the separate annular elements (j=1 to i) by the usual method:

$$\tau_o = \frac{1}{2}(\sigma_1(j) - \sigma_3(j)) \quad [27]$$

where $\boldsymbol{\sigma_1}$(j), $\boldsymbol{\sigma_2}$(j), and $\boldsymbol{\sigma_3}$(j) are the maximum, intermediate, and minimum principal stresses of the j^{th} annular element at time **t**(j) determined from values for $\boldsymbol{\sigma_z^{SiO2}}$(j), $\boldsymbol{\sigma_r^{SiO2}}$(j), and $\boldsymbol{\sigma_\theta^{SiO2}}$(j).

E. Determination of Relaxed Principal Stresses from Relaxed Shear Stress

Calculation of the relaxation of the principal stresses from relaxation of the shear stress $\boldsymbol{\tau_o}$ to $\boldsymbol{\tau}$(t) in equation [26] is complicated by the presence of both tensile and compressive principal stresses. It is therefore also useful to designate principal stresses by their rank in absolute value as $\boldsymbol{^1\sigma}$ (j) , $\boldsymbol{^2\sigma}$ (j), and $\boldsymbol{^3\sigma}$(j), and to define:

$$\delta[\sigma(j)] = \begin{cases} 1 & \sigma(j) > 0 \\ -1 & \sigma(j) < 0 \end{cases} \quad [28]$$

A boundary condition is $\boldsymbol{\sigma_r^{SiO2}}$(1) = 0, but $\boldsymbol{\sigma_r^{SiO2}}$(j>1) will have a small negative value (compression) if $\boldsymbol{\sigma_z^{SiO2}}$(j>1) and $\boldsymbol{\sigma_\theta^{SiO2}}$(j>1) are positive (tension), or a positive value if the other principal stresses are negative. Since the scale is free to expand in the radial direction, volume is not conserved,

and decomposition of the stress tensor into hydrostatic and deviatoric components, as used for some growth stress calculations,[13-14] is not useful because the hydrostatic pressure can change with relaxation. In almost all cases $\boldsymbol{\sigma}_r^{SiO2}(j)$ will be ${}^3\boldsymbol{\sigma}$ (j), but there are some exceptions when $\boldsymbol{\sigma}_z^{SiO2}(j)$ or $\boldsymbol{\sigma}_\theta^{SiO2}(j)$ are changing from compressive (negative) to tensile (positive) and are therefore ${}^3\boldsymbol{\sigma}$ (j) for a relatively short period of time. The different relationships between $\boldsymbol{\sigma}_{1,2,3}(j)$ and ${}^{1,2,3}\boldsymbol{\sigma}(j)$ are shown in figure 3, and require differences in the way new principal stresses $[\sigma(j)']$ are calculated after shear stress relaxation. Two methods are employed. The first assumes that only ${}^1\boldsymbol{\sigma}(j)$ will relax, until it reaches the value for ${}^2\boldsymbol{\sigma}(j)$, at which point both relax. This method is best suited for high $\boldsymbol{\tau}$ where η [23] is not Newtonian, and is later referenced as the "High τ Method". $\boldsymbol{\sigma}_r^{SiO2}(j)$ is a boundary condition unless $|\boldsymbol{\sigma}_r^{SiO2}(j)| \leq |\boldsymbol{\sigma}_z^{SiO2}(j)|$ & $|\boldsymbol{\sigma}_\theta^{SiO2}(j)|$, where the boundary condition becomes 0 for all stresses. For principal stresses of type (${}^1\boldsymbol{\sigma}_1$, ${}^2\boldsymbol{\sigma}_2$, ${}^3\boldsymbol{\sigma}_3$) or (${}^3\boldsymbol{\sigma}_1$, ${}^2\boldsymbol{\sigma}_2$, ${}^1\boldsymbol{\sigma}_3$):

If $2\tau(j) > |{}^2\sigma(j) - {}^3\sigma(j)|$:

$$\begin{aligned} {}^1\sigma(j)' &= {}^3\sigma(j) + 2\delta[{}^1\sigma(j)]\tau \\ {}^2\sigma(j)' &= {}^2\sigma(j) \\ {}^3\sigma(j)' &= {}^3\sigma(j) \end{aligned} \quad [29]$$

If $2\tau(j) < |{}^2\sigma(j) - {}^3\sigma(j)|$ & $\delta[{}^2\sigma(j)] = \delta[{}^3\sigma(j)]$:

$$\begin{aligned} {}^1\sigma(j)' &= {}^3\sigma(j) + 2\delta[{}^1\sigma(j)]\tau \\ {}^2\sigma(j)' &= {}^3\sigma(j) + 2\delta[{}^1\sigma(j)]\tau \\ {}^3\sigma(j)' &= {}^3\sigma(j) \end{aligned} \quad [30]$$

If $2\tau(j) < |{}^2\sigma(j) - {}^3\sigma(j)|$ & $\delta[{}^2\sigma(j)] \neq \delta[{}^3\sigma(j)]$ & $\tau(j) > |{}^3\sigma|$:

$$\begin{aligned} {}^1\sigma(j)' &= {}^3\sigma(j) + 2\delta[{}^1\sigma(j)]\tau \\ {}^2\sigma(j)' &= {}^3\sigma(j) + 2\delta[{}^1\sigma(j)]\tau \\ {}^3\sigma(j)' &= {}^3\sigma(j) \end{aligned} \quad [31]$$

If $2\tau(j) < |{}^2\sigma(j) - {}^3\sigma(j)|$ & $\delta[{}^2\sigma(j)] \neq \delta[{}^3\sigma(j)]$ & $\tau(j) < |{}^3\sigma|$:

$$\begin{aligned} {}^1\sigma(j)' &= \delta[{}^1\sigma(j)]\tau \\ {}^2\sigma(j)' &= \delta[{}^2\sigma(j)]\tau \\ {}^3\sigma(j)' &= \delta[{}^3\sigma(j)]\tau \end{aligned} \quad [32]$$

For all other principal stresses:

If $\tau(j) > |{}^2\sigma(j)|$:

$$\begin{aligned} {}^1\sigma(j)' &= {}^2\sigma(j) + 2\delta[{}^1\sigma(j)]\tau \\ {}^2\sigma(j)' &= {}^2\sigma(j) \\ {}^3\sigma(j)' &= {}^3\sigma(j) \end{aligned} \quad [33]$$

If $|{}^2\sigma(j)| > \tau(j) > |{}^3\sigma(j)|$:

$$\begin{aligned} {}^1\sigma(j)' &= \delta[{}^1\sigma(j)]\tau \\ {}^2\sigma(j)' &= \delta[{}^2\sigma(j)]\tau \\ {}^3\sigma(j)' &= {}^3\sigma(j) \end{aligned} \quad [34]$$

If $\tau(j) < |{}^3\sigma(j)|$:

$$\begin{aligned} {}^1\sigma(j)' &= \delta[{}^1\sigma(j)]\tau \\ {}^2\sigma(j)' &= \delta[{}^2\sigma(j)]\tau \\ {}^3\sigma(j)' &= \delta[{}^3\sigma(j)]\tau \end{aligned} \quad [35]$$

This method is consistent with radial expansion at a free surface with minimization of strain energy through minimization of ${}^1\boldsymbol{\sigma}(j)^2 + {}^2\boldsymbol{\sigma}(j)^2 + {}^3\boldsymbol{\sigma}(j)^2$. The relaxed values of ${}^1\boldsymbol{\sigma}(j)'$, ${}^2\boldsymbol{\sigma}(j)'$, and ${}^3\boldsymbol{\sigma}(j)'$ are reassigned to $\boldsymbol{\sigma}_z^{SiO2}(j)$, $\boldsymbol{\sigma}_r^{SiO2}(j)$, and $\boldsymbol{\sigma}_\theta^{SiO2}(j)$.

The second method assumes that viscosity is Newtonian and that the rate of $\boldsymbol{\sigma}_\theta(j)$and $\boldsymbol{\sigma}_z(j)$ relaxation is proportional to their difference with $\boldsymbol{\tau}(t)/\boldsymbol{\tau}_o$ and $\boldsymbol{\sigma}_r(j)$, which is a boundary condition and does not change, being zero at the SiO_2 surface and near zero elsewhere. This method is best suited for high temperatures and low shear stresses where $\boldsymbol{\eta}$ is Newtonian, and is later referenced as the "Low τ Method". $\boldsymbol{\sigma}_\theta(j)'$ and $\boldsymbol{\sigma}_z(j)'$ can be determined by solution of:

$$\begin{bmatrix} \sigma_\theta(j)' & 0 & 0 \\ 0 & \sigma_z(j)' & 0 \\ 0 & 0 & \sigma_r(j) \end{bmatrix} = \frac{\tau(t)}{\tau_o} \begin{bmatrix} \sigma_\theta(j) - \sigma_r(j) & 0 & 0 \\ 0 & \sigma_z(j) - \sigma_r(j) & 0 \\ 0 & 0 & \sigma_r(j) \end{bmatrix} + \begin{bmatrix} \sigma_r(j) & 0 & 0 \\ 0 & \sigma_r(j) & 0 \\ 0 & 0 & \sigma_r(j) \end{bmatrix} \quad [36]$$

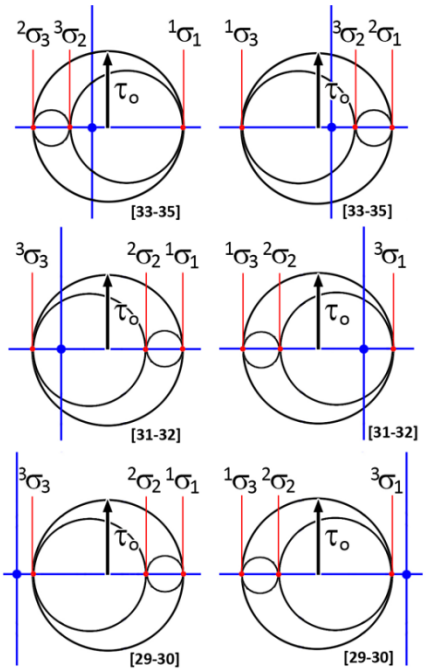

Fig. 3 The relationships between the magnitudes (σ_i) and absolute value magnitudes ($^i\sigma$) of the principal growth stresses that are used to calculate principal stress relaxation from shear stress relaxation in [29] – [35].

At very low principal stresses, where $|\sigma_r^{SiO2}(j)| \geq |\sigma_z^{SiO2}(j)|$ & $|\sigma_\theta^{SiO2}(j)|$ and they are opposite in sign, $|\sigma_z^{SiO2}(j)|$ and $|\sigma_\theta^{SiO2}(j)|$ increase, and this method is therefore inconsistent with minimization of strain energy. However, this condition can only occur very briefly when $\sigma_z^{SiO2}(j)$ and $\sigma_\theta^{SiO2}(j)$ change from compressive to tensile from radial displacement of the scale, described next.

F. Radial Displacement and Hoop Stress Generation in Scale

Relaxation expands the SiO_2 scale radially. The individual radial displacement of the jth layer ($\mathbf{u_r(j)}$) is:

$$u_r(j) = \frac{\Omega_{SiO_2}}{\Omega_{SiC}\left(1 + \varepsilon_z^{SiO2}(j) + \varepsilon_\theta^{SiO2}(j) + \varepsilon_z^{SiO2}(j)\varepsilon_\theta^{SiO2}(j)\right)} - 1 \quad [37]$$

where

$$\varepsilon_z^{SiO2}(j) = \frac{1}{E_{SiO_2}}\left[\sigma_z^{SiO2}(j) - \upsilon_{SiO_2}\left(\sigma_\theta^{SiO2}(j) + \sigma_r^{SiO2}(j)\right)\right] \quad [38]$$

$$\varepsilon_\theta^{SiO2}(j) = \frac{1}{E_{SiO_2}}\left[\sigma_\theta^{SiO2}(j) - \upsilon_{SiO_2}\left(\sigma_z^{SiO2}(j) + \sigma_r^{SiO2}(j)\right)\right] \quad [39]$$

The radial displacement of the j^{th} outer layer is equal to the sum of the radial displacements of all the younger layers (i-j-1) beneath it. This adds hoop strain ($\varepsilon_\theta^{SiO2}$) to outer, older layers as they are displaced radially outward and forced to a larger circumference (Fig. 1). The new hoop strain in each layer can be calculated from the sum:

$$\varepsilon_\theta^{SiO2}(j) = \varepsilon_\theta^{SiO2}(j) + \sum_j^i u_r(j)\frac{b(j-1) - b(j)}{b(j)} \quad [40]$$

where

$$w(i) - w(i-1) = \sum_{i-1}^{i} u_r(i)\left(b(i-1) - b(i)\right) \quad [41]$$

for complete relaxation of the youngest layer.

G. Recalculation of Elastic Stress in the Scale and SiC Fiber after Radial Displacement

The stress in each SiO_2 layer can then be recalculated from the new $\varepsilon_\theta^{SiO2}$ by solving the three strain compatibility equations for the three principal stresses:

$$\varepsilon_z^{SiO2}(j) = \frac{1}{E_{SiO_2}}\left[\sigma_z^{SiO2}(j) - \upsilon_{SiO_2}\left(\sigma_\theta^{SiO2}(j) + \sigma_r^{SiO2}(j)\right)\right] \quad [42]$$

$$\varepsilon_\theta^{SiO2}(j) = \frac{1}{E_{SiO_2}}\left[\sigma_\theta^{SiO2}(j) - \upsilon_{SiO_2}\left(\sigma_z^{SiO2}(j) + \sigma_r^{SiO2}(j)\right)\right] \quad [43]$$

$$\varepsilon_r^{SiO2}(j) = \frac{1}{E_{SiO_2}}\left[\sigma_r^{SiO2}(j) - \upsilon_{SiO_2}\left(\sigma_\theta^{SiO2}(j) + \sigma_z^{SiO2}(j)\right)\right] \quad [44]$$

The revised principal stresses in the SiC fiber can then be calculated. The axial stress σ_z^{SiC} is computed from the total force exerted by the SiO_2 layers which is the sum of the axial stress in each annular SiO_2 element × area of that element:

$$\sigma_z^{SiC}(i) = -\sum_{j=1}^{i-1} \frac{\sigma_z^{SiO2}(j)[2c(i)(w(j) - w(j-1) + w(j)^2 - w(j+1)^2]}{b(i)^2} \quad [45]$$

The revised radial and hoop stress in the SiC fiber can be computed in a similar manner, by computing the net pressure (p_n) from the sum of the pressures in each annular layer:

$$\sigma_r^{SiC}(i) = \sigma_\theta^{SiC}(i) = -p_n = -\sum_{j=1}^{i-1} \sigma_\theta^{SiO2}(j) \frac{w(j) - w(j-1)}{b(i)} \quad [46]$$

These revised stresses are changed incrementally for strain compatibility and stress relaxation as the program loops back to equations [1 - 41] as the next layer i is considered. For SiC oxidation when **w(i)** << **b(i)**, the stress in SiO_2 is much larger than that in SiC and can be neglected for approximate calculations.

III. Results and Discussion

A. General

Growth stress calculations were done using equations [1-46] in a Mathematica™ program. Calculations were done with 50 to 2000 layers (i = 50 to 2000). Variations in calculations were usually insignificant for i > 100. A value of i = 500 was chosen as an optimal trade-off between precision and calculation speed.

Calculations were done for oxidation of Hi-Nicalon™-S SiC fiber for amorphous scales of 10, 100, 1000, and 3000 nm thickness (**w**) at 700, 800, 900, 1000, 1100, 1200, and 1300°C. The Deal-Grove oxidation kinetics for this fiber have been reported for dry air between 700 and 1300°C with $\mathbf{A_o}$ = 6.5 × 10^{-4} m, $\mathbf{B_o}$ = 1.2 × 10^{-8} m^2/s, $\mathbf{Q_A}$ = 111 kJ/mol, and $\mathbf{Q_B}$ = 249 kJ/mol.[5-6] The fiber radius ($\mathbf{b_0}$) is 6.1 μm. The molar volumes for SiC ($\mathbf{\Omega_{SiC}}$) and amorphous SiO_2 ($\mathbf{\Omega_{SiO2}}$) are 27.34 cm^3 and 12.46 cm^3, respectively. The Young's modulus (**E**) and Poisson's ratio (**ν**) values used for SiC and SiO_2 were $\mathbf{E_{SiC}}$ = 400 GPa, $\mathbf{\nu_{SiC}}$ = 0.157, $\mathbf{E_{SiO2}}$ = 70 GPa, and $\mathbf{\nu_{SiO2}}$ = 0.17. The shear modulus value used for silica (**G**) was 34 GPa. The continuous variation in growth stress with change in fiber radius was examined by calculations using $\mathbf{b_0}$ = 3 μm and $\mathbf{b_0}$ = →∞ (1 km).

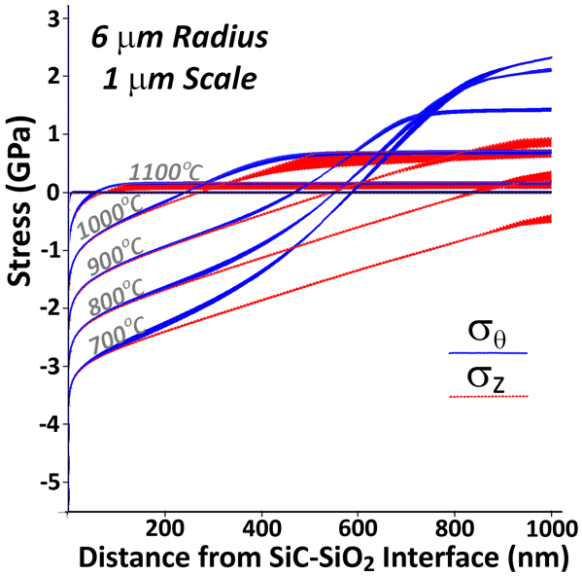

Fig. 4. Hoop stress (σ_θ) and axial stress (σ_z) for a 1 μm thick scale on a Hi-Nicalon™-S (6 μm radius) fiber calculated using the "High τ Method" [29-35] and "Low τ Method" [36]. Differences in calculated values between the two methods are small. Compressive values are negative.

General features for hoop stress (σ_θ) and axial stress (σ_z) are evident in figure 4 for a 1 μm thick scale on a Hi-Nicalon™-S (6 μm radius) fiber. Qualitatively, these results are most similar to those of Delph for elastic-viscoplastic scales during silicon oxidation.[20] Compressive elastic stress of ~-25 GPa for σ_θ and σ_z is rapidly relaxed by the Eyring model [23] for SiO_2 glass viscosity (**η**) to ~-3 GPa at 700°C and -1 GPa at 1000°C just 10 nm away from the SiC-SiO_2 interface. This quickly reduces the problem to one similar to unidirectional radial expansion with a residual "intrinsic strain" parallel to the SiC-SiO_2 interface. However, this "intrinsic strain" is T and t dependent,

and the calculations done using unidirectional radial expansion show only tensile σ_θ, with no transition from compressive to tensile stress. [20, 25]

At the scale surface, σ_θ is ~2 GPa (tension) at 700° and 800°C, and σ_z is ~1 GPa (tension) at 700°C. σ_z is driven towards tensile values by the Poisson effect from radial expansion that creates tensile σ_θ. Viscous stress relaxation reduces all growth stresses to < 100 MPa at 1100°C and < 10 MPa at 1300°C everywhere in the SiO_2 scale except the region immediately adjacent to the SiC-SiO_2 interface.

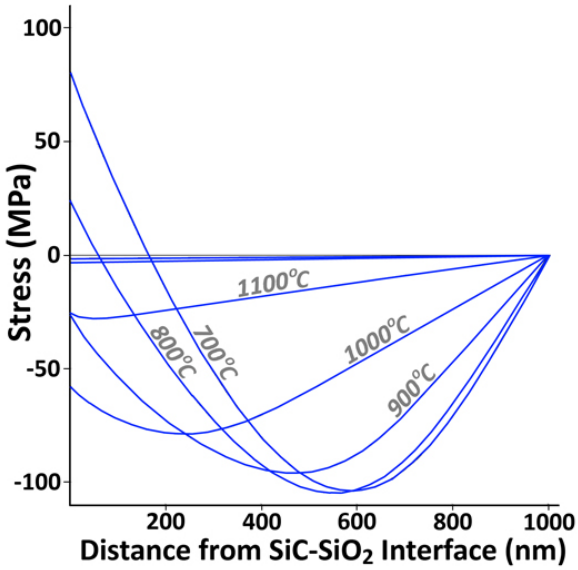

Fig. 5. Radial stress (σ_r) for a 1 μm thick scale on a Hi-Nicalon™-S (6 μm radius) fiber calculated using the "High τ Method" [29-35].

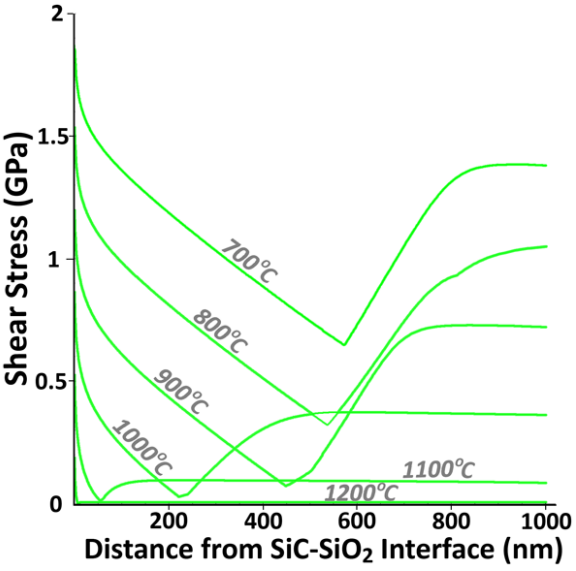

Fig. 6. Shear stress (τ) for a 1 μm thick scale on a Hi-Nicalon™-S (6 μm radius) fiber calculated using the "High τ Method" [29-35].

Radial stress (σ_r) calculated by the "High τ Method" [29-35] for a 1 μm thick scale on a Hi-Nicalon™-S (6 μm radius) fiber is shown in figure 5 and shear stress (τ)is shown in figure 6. Compressive σ_r up to ~100 MPa is present in the center of the scale at 700° - 900°C. This is a consequence of tensile σ_θ at the scale surface. At 700° - 800°C σ_r goes tensile at the SiC-SiO_2 interface, which is a consequence of the high compressive σ_θ near that interface.

τ of ~12 GPa is rapidly relaxed to ~ 2 GPa at 700°C and 500 MPa at 1100°C just 10 nm away from the SiC-SiO_2 interface (Fig. 6). It continues to decrease as compressive σ_z and σ_θ decreases away from the SiC-SiO_2 interface until σ_θ becomes tensile, at which point τ increases towards the SiO_2 surface, reaching surface values close to 1.5 GPa at 700°C and 300 MPa at 1000°C. The shear stress minimum is ~ 600 nm from the SiC-SiO_2 interface at 700°C, 200 nm at 1000°C, and ~50 nm at 1100°C. Note that a 1 μm scale takes ~10^9 s to form at 700°C and ~10^6 s to form at 1000°C, so the latter is of more practical interest.

The practical use of the growth stress calculation method is likely to be limited by knowledge of accurate values for amorphous silica viscosity. Unlike silicon oxidation, silica scales formed during SiC oxidation incorporate carbon.[49-52] Network carbon in amorphous SiO_2 stiffens the network structure, making it more viscous and less permeable to O_2.[45, 53-54] However, SiO_2 viscosity may be reduced by incorporation of the Cl (620 ppm), S (52 ppm), Ca (45 ppm), Na (35 ppm), and Fe (27 ppm) impurities in Hi-Nicalon™-S fiber.[6]

B. Comparison of Methods for Calculation of Relaxed Principal Stresses

Two methods for calculation of the relaxed principal stresses from the relaxed shear stress were developed (equations [29-36]). These methods are compared for a 1000 nm thick amorphous SiO_2 scale on a 6 μm radius Hi-Nicalon™-S fiber at 700° - 1300°C in figure 4. The differences between the methods are illustrated by the thickness of the colored lines. For σ_θ there is little difference between the two methods. The "Low τ Method" [36] finds σ_θ values slightly lower in absolute value than the "High τ Method" [29-35]. In the compressive stress regions of the scale (negative values, close to the SiC-SiO_2 interface) the calculated values for axial stress (σ_z) are nearly identical. Close to the surface it is higher (more tensile) at 700° and 800°C and lower (less tensile) for higher temperatures. At 1100°C and higher, stresses are rapidly relaxed by viscous flow. There is a 2× relative difference in calculated values of σ_z between the two methods, but the absolute difference is small because stresses are low (~ 100 MPa) and highly relaxed by viscous flow. Since high scale stresses

are generally of more interest for structural SiC fibers, further calculations are presented from the "High τ Method".

C. Variation with Scale Thickness and Fiber Radius

Calculations for 3 μm radius ($\mathbf{b_0}$), 6 μm radius, and a flat plate for 10 nm, 100 nm, and 1 μm thick ($\mathbf{w}$) scales at 700 - 1300°C are shown in figure 7. The continuous change of σ_θ and σ_z with change in $\mathbf{b_0}$

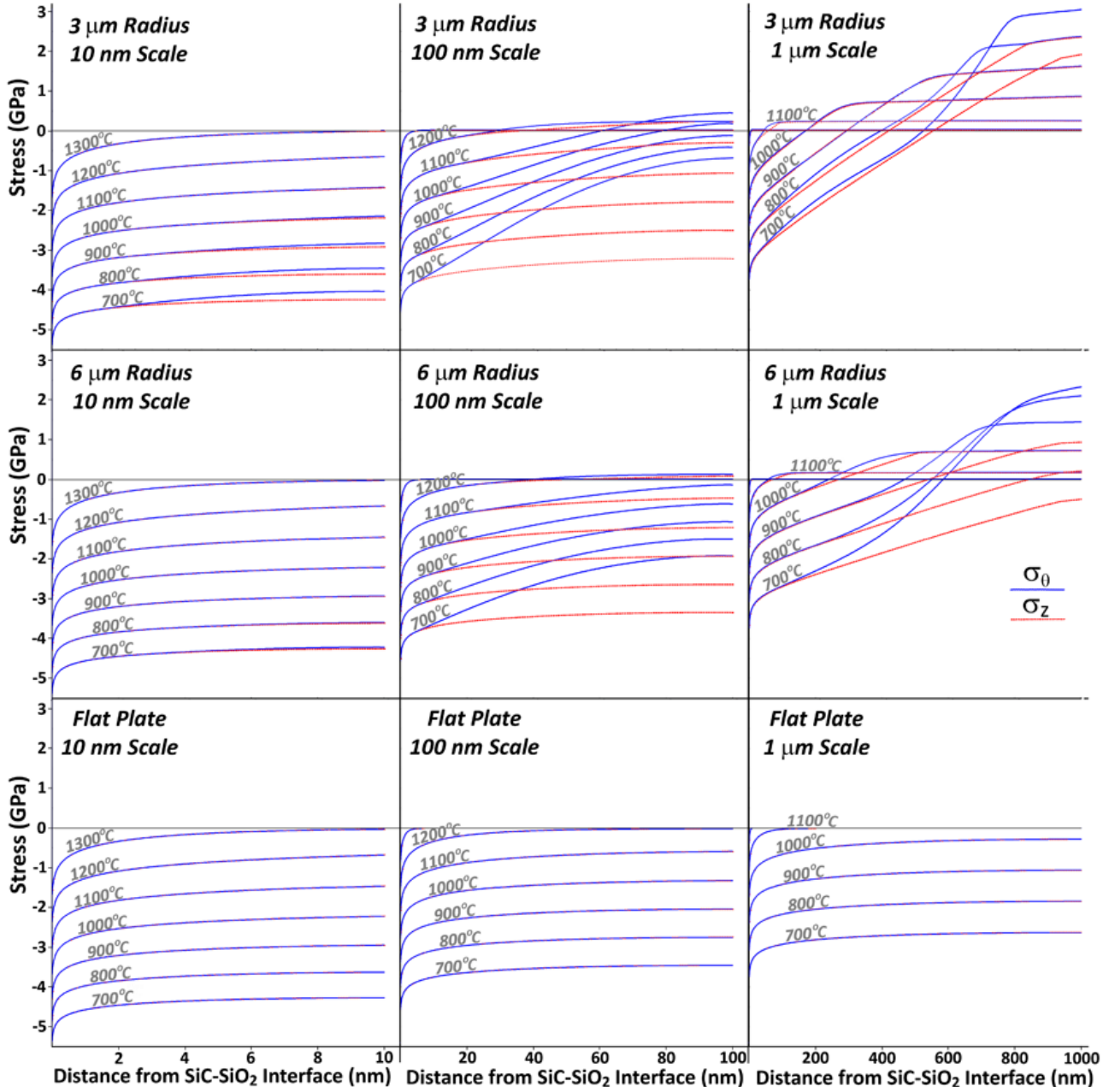

Fig. 7. Hoop (σ_θ) and axial oxidation growth stress (σ_z) levels as a function of position in the SiO_2 scale for SiC flat plates and fibers with 6 and 3 μm radius ($\mathbf{b_0}$). Results for $\mathbf{w}$ = 10 nm, 100 nm, and 1 μm thick scales are shown for temperatures of 700°, 800°, 900°, 1000°, 1100°, 1200°, and 1300°C. The continuous change in both σ_θ and σ_z with the variables of scale position, temperature ($\mathbf{T}$), scale thickness ($\mathbf{w}$), and fiber radius ($\mathbf{b_0}$) is evident.

and $\mathbf{w}$ at 700°C to 1300°C throughout the scale is evident. For flat plates of $\sigma_\theta = \sigma_z$, and stress is always compressive. Growth stress for $\mathbf{w}$ = 10 nm is very similar to that of a flat plate for $\mathbf{b_0}$ = 3 and 6 μm.

For a 3 μm radius fiber, tensile σ_θ develops at the scale surface at temperatures over 950°C for **w** = 100 nm and reaches values of 400 MPa at 1100°C. Tensile σ_z does not develop until **T** > 1150°C and reaches 100 MPa at 1200°C. For a 6 μm radius fiber, tensile stress does not develop at the scale surface until temperatures close to 1200°C are reached; maximum tensile σ_θ and σ_z of 100 MPa forms at 1200°C. For both b_0 = 3 and 6 μm with **w** = 100 nm, σ_z is generally much more compressive than σ_θ, except at the highest temperatures stresses are almost completely relaxed.

The results for **w** = 1 μm scales with b_0 = 6 μm were discussed in the previous section. Maximum tensile σ_θ reaches 2.3 GPa and 3 GPa for b_0 = 6 and 3 μm, respectively, at 700°C. Maximum tensile σ_z reaches 1 GPa (900°C) and 2.2 GPa (800°C) for b_0 = 6 and 3 μm, respectively. Much larger fractions of the scale are under tensile stress for a 1 μm thick scale in comparison to a 100 nm thick scale.

D. Surface Stress

For structural SiC fibers the residual stress at the scale surface is of great interest. Tensile stress promotes formation of cracks that can degrade fiber strength.[5-6] Compressive stress may have the opposite effect. The stress values at maximum distance from the SiC-SiO_2 interface in figure 7 are the surface stresses (right hand side of each plot). Calculations for the hoop stress (σ_θ) and axial stress (σ_z) at the scale surface are mapped as a function of temperature (**T**) and scale thickness (**w**) in figures 8-10

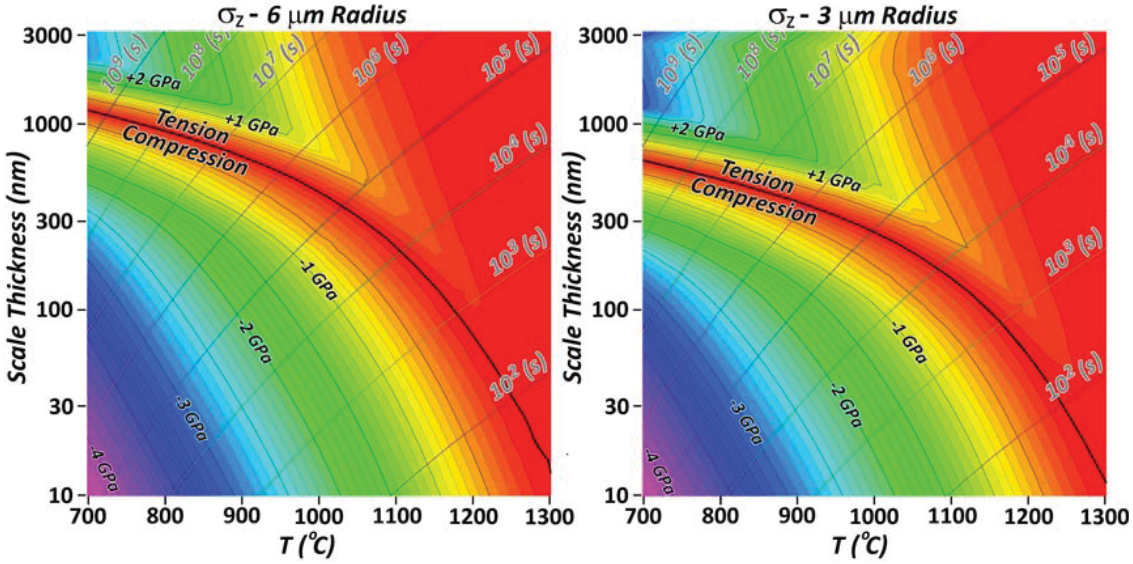

Fig. 8. Axial stress (σ_z) at the SiO_2 scale surface as a function of scale thickness and oxidation temperature for 6 and 3 μm radius SiC fibers. Oxidation time isochrones are also shown.

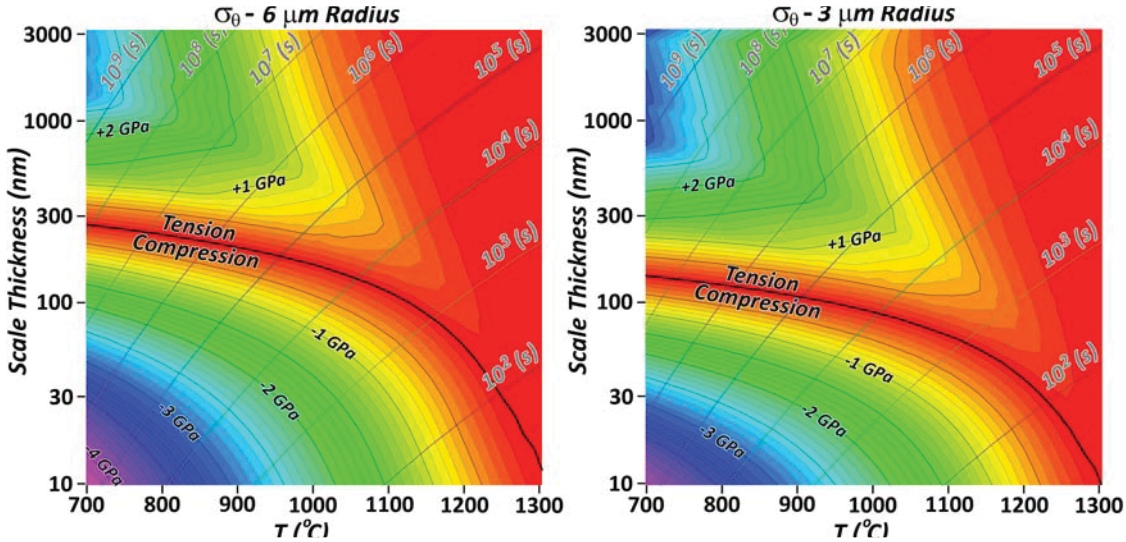

Fig. 9. Hoop stress (σ_θ) at the SiO_2 scale surface as a function of scale thickness and oxidation temperature for 6 and 3 μm radius SiC fibers. Oxidation time isochrones are also shown.

for flat plates, 6 μm radius fibers, and 3 μm radius fibers. These plots clearly distinguish tensile and compressive regions, and also show logarithmic time isochrones in seconds.

The tensile stress maximum forms at smaller scale thicknesses as temperature increases. This maximum is the greatest practical concern for structural SiC fibers. The plots illustrate T-t windows that should be avoided. For example, a tensile σ_z of ~500 MPa forms for a scale of ~ 600 nm thickness at 1050°C in 10^5 seconds (~ 1 day) during oxidation of a 6 μm radius fiber in dry air (Fig. 8). For a 3 μm radius fiber this maximum is ~750 MPa. Longer oxidation times would decrease, rather than increase, this stress. Much higher tensile stresses are possible at lower temperatures, but require much longer to form, and will form for thicker rather than thinner scales. These high tensile stresses may impact fiber strength at temperature. They are larger than the compressive thermal stresses that will develop in the SiO_2 scale during cool down (~300 MPa), and so may impact room temperature strength as well.

The maximum tensile σ_θ that forms at 1050°C is ~600 and 900 MPa for 6 and 3 μm radius fibers, respectively (Fig. 9). This stress maximum occurs at a significantly lower scale thickness and shorter time than the σ_z maximum (Fig. 8). Tensile σ_θ stresses have been suggested to cause axial cracking of scale during oxidation, rendering the scale non-passivating.[5-6] Calculations for a flat plate, where all stresses are compressive, are shown in figure 10 for comparison.

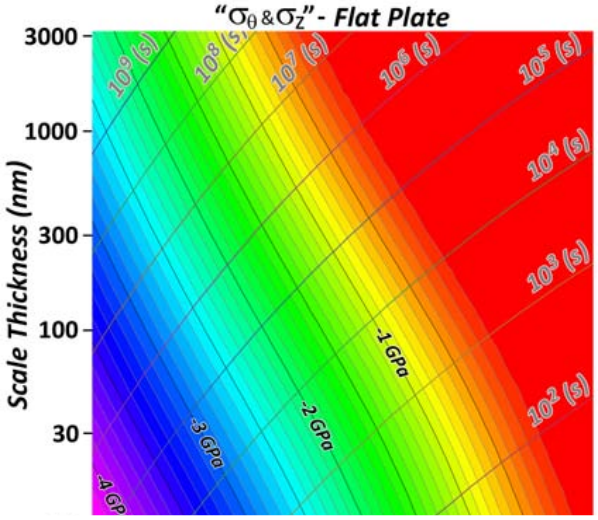

Fig. 10. Stress ($\sigma_\theta = \sigma_z$) at the SiO_2 scale surface as a function of scale thickness and oxidation temperature. Oxidation time isochrones are also shown.

E. Steady-State Tensile Stress

A near "steady-state" develops for tensile stress at **T** ≥ 1200°C for **w** = 100 nm for both $\mathbf{b_0}$ = 3 and 6 μm (Fig. 7). At lower temperatures, greater scale thickness is required to reach steady-state. A **w** > ~1 μm is required for **T** ≥ 1000°C. The tensile σ_θ and σ_z values are nearly equal, with little change for significant distances beneath the scale surface (Fig. 7), but the scale thickness (time) required to reach steady-state is longer for σ_z because it is driven to tensile values by the Poisson effect from σ_θ. For shear stress $\tau < \tau_c$ of 100 MPa [23] where a stress–free viscosity (η_o) [24] is applicable, a simple expression for the steady-state hoop stress [σ_θ(ss)] can be derived. The rate at which scale thickness (δ) is increased from the oxidation volume increase is:

$$\frac{d\delta}{dt} = \frac{B}{w}\left(\frac{1}{\Omega} - 1\right) \qquad [47]$$

If σ_r is negligible, the shear stress is half the hoop stress, and the rate at which hoop strain (ε_θ) develops in the outer scale is:

$$\frac{d\varepsilon_\theta}{dt} = \frac{\tau}{\eta_o} = \frac{\sigma_\vartheta(ss)}{2\eta_o} = \frac{\frac{d\delta}{dt}}{b} \qquad [48]$$

[47] and [48] can be solved for the steady-state hoop stress σ_θ(ss):

$$\sigma_\theta\,(ss) = \frac{2B\left(\frac{1}{\Omega} - 1\right)\eta_o}{wb} \qquad [49]$$

For τ > 100 MPa the stress dependence of viscosity is significant, and [23] must be substituted for η_o, giving:

$$\sigma_\theta\,(ss) = -2\tau_c \mathbf{Csch}\left[\frac{bw\tau_c\Omega}{B\eta_o(\Omega-1)}\right]^{-1} \qquad [50]$$

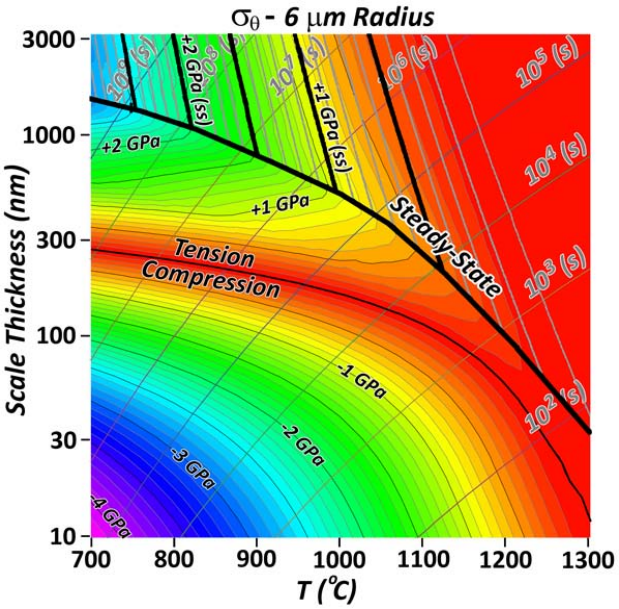

Fig. 11. The plot for surface stress in Fig. 9 for $\mathbf{b_o}$ = 6 μm, with predictions for the steady-state region from [50] superimposed.

Predictions for steady-state σ_θ tensile stress from [50] for a 6 μm radius fiber are shown in figure 11. High temperature (> 1150°C) steady-state stress value predictions are high, but at lower temperatures the prediction is close to calculated values. A steady state develops in ~2 minutes at 1300°C, 3 hours at 1100°C, and in ~100 days at 900°C. The predictions for σ_z are the same as those for σ_θ, except the times to reach steady state are longer (Fig. 8). For smaller radius fibers the time to reach steady-state is also shorter.

By expanding [49] with the Arrhenius expressions for **B** and η_o, the steady-state tensile stress decrease with increasing temperature is evident when **Q** > $\mathbf{Q_b}$; the scale viscosity decreases faster with an increase in temperature than the oxidation rate:

$$\sigma_\theta\,(ss) = \frac{2B_oC_oe^{\frac{Q-Q_b}{RT}}\left(\frac{1}{\Omega}-1\right)}{wb} \qquad [51]$$

This suggests that if materials exist for which **Q** < $\mathbf{Q_b}$, a counterintuitive increase in tensile growth stress with increase in oxidation temperature is expected – the oxidation rate, and growth stress generation associated with it, will increase faster than the rate at which viscosity decreases.

F. Crystalline Scale

SiO_2 scale crystallization kinetics have been measured for Hi-Nicalon™-S SiC fiber; crystallization begins after ~ 100 hours at 1000°C or 1 hour at 1300°C, when scales are roughly 500 nm and 100 nm thick, respectively.[5-6] Unfortunately, SiC oxidation kinetics for crystalline scales (cristobalite and tridymite) are not well characterized, and there is even less data on creep rates and/or viscosities. However, it is clear that the oxidation kinetics for crystalline scales are slower.[5-6] Some kinetic data suggests that crystalline scale thicknesses are ~1/3 those for amorphous scales.[55-56] Temperature dependence was not reported, so to a first approximation it is assumed that $\mathbf{B_o}$ is an order of magnitude smaller ($\mathbf{B_o}$ = 1.2 × 10^{-9} m^2/s) and other Deal-Grove parameters are unchanged. Limited data for creep rates for cristobalite refractories suggests that at 1550° - 1650°C creep is negligible at very low stress (0.2 to 0.6 MPa), but further quantification was not possible.[36-38]

To explore the possible effects of crystallization on growth stress, we assume that cristobalite viscosity is four orders of magnitude higher than that of amorphous silica at all temperatures: $\mathbf{C_o}$ = 3.8 × 10^{-9} Pa·s [24]. Calculations are done for a 1 μm thick scale at 1100°C, and for cases where crystallization occurs when the scale is 100 nm thick, 500 nm thick, and 900 nm thick (Fig. 12). These thicknesses set the value for $\mathbf{x_i}$ in [1]. Crystallization rates are very rapid compared to scale growth rates.[5-6] We assume that during crystallization all stresses in the amorphous SiO_2 are eliminated and are not transferred into the crystalline product. Calculations for an SiO_2 glass (Fig. 7) are included for comparison.

At 1100°C, σ_θ and σ_z are tensile, < 200 MPa, and in steady-state throughout most of the scale (Fig. 12). For early scale crystallization (x_i = 100 nm), σ_θ is 1.6 GPa (tension) at the scale surface, and σ_z is 450 MPa (tension). For $\mathbf{x_i}$ = 500 nm, these values are 700 MPa and 150 MPa, respectively, but a higher tensile σ_θ of 1.5 GPa is present at **x** = 500 nm, with a sharp transition to high compressive stress at

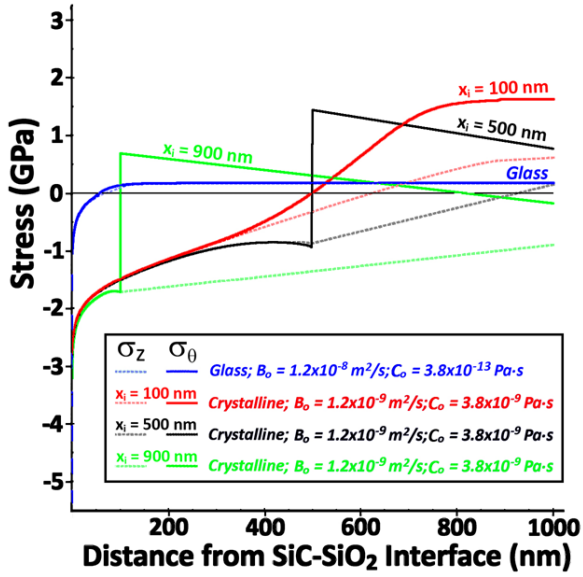

Fig. 12. Hoop (σ_θ) and axial growth stress (σ_z) levels after oxidation at 1100°C as a function of position in a crystalline SiO_2 scale for SiC fibers with 6 μm radius ($\mathbf{b_0}$). Stress after scale crystallization at $\mathbf{x_i}$ = 100, 500, and 900 nm is calculated, as well as glass for comparison.

the point in the scale at which crystallization occurred. For $\mathbf{x_i}$ = 900 nm the scale has spent a relatively short time growing in the crystalline state. Surface stresses are compressive, but tensile σ_θ of 700 MPa develops at **x** = 100 nm.

As expected, much lower scale viscosities cause much higher stresses. Cracks that form during oxidation in cristobalite and tridymite scales, but not in amorphous scales,[5-6] can clearly be a consequence of the much higher tensile surface stresses (> 1 GPa) that may develop in crystalline SiO_2 scales. Porosity present in the centers of crystalline scales might also be inferred to be a consequence of hydrostatic tension that develops at the point in the scale at which crystallization occurred. Crystalline SiO_2 will deform by dislocation plasticity at high τ; mechanisms implicit in the Eyring model for glass no longer apply. There is evidence for intense dislocation plasticity in crystalline SiO_2 scale near the SiC-SiO_2 interface.[5-6] The 20 nm of SiO_2 adjacent to SiC will have τ > 1 GPa, which is more than enough for domination of creep by dislocation-based mechanisms.[57]

G. Effects of Stress on Oxidation Rate

The retardation of silicon oxidation by compressive growth stress and externally applied stress, and the enhancement by externally applied tensile stress was briefly mentioned.[8, 12, 20, 24-25, 29-31] Some data for oxidation enhancement by tensile stress also exists for SiC.[32] Recent work on SiC fiber oxidation finds the oxidation rates tend to be higher than those observed for bulk SiC.[5-6] There was speculation that this could be a SiC substrate geometry effect, related to the development of tensile stress in the fiber scale.

The usual method for handling stress effects on oxidation kinetics is to assume a pressure (**p**) effect on the parabolic rate constant **B**:

$$B(p) = Be^{pV_d/kT} \quad [52]$$

where $\mathbf{V_d}$ is an activation volume, calculated to be 7.5×10^{-29} m^3 for silicon oxidation,[12, 20, 25] and pressure is:

$$p = \frac{1}{3}(\sigma_\theta + \sigma_z + \sigma_r) \quad [53]$$

The pressure clearly varies from high negative values (hydrostatic compression) at the SiC-SiO_2 interface to lower values at the surface; these can reverse sign be in hydrostatic tension for thick scales at low temperatures (Fig. 7).

A first-order correction for the relative effects of growth stress in flat-pale and cylindrical geometries is attempted by calculating the average self-pressure ($\mathbf{p_{av}}$) in the SiO_2 scale throughout its thickness, as a function of total scale thickness (**w**), temperature, and fiber radius. This is done by summing the pressure – scale volume product for each scale increment and normalizing by the scale volume:

$$p(av) = \frac{1}{c_i^2 - b_i^2} \sum_{j=1}^{i} p(b_j^2 - b_{j-1}^2) \quad [54]$$

The average pressure ($\mathbf{p_{av}}$) was calculated for 6 and 3 μm radius fibers (Fig. 13) as a function of total scale thickness from 10 to 3000 nm and temperature from 700° to 1300°C. Average pressures of

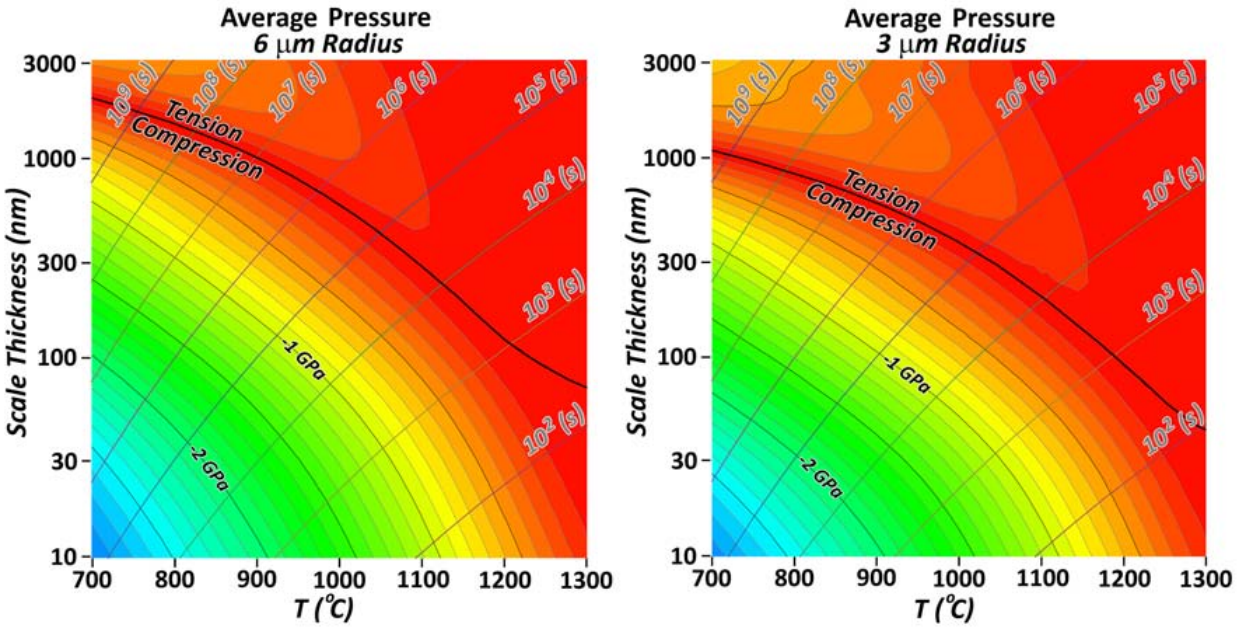

Fig. 13. Average SiO_2 scale self-pressure ($\mathbf{p_{av}}$) for 6 and 3 μm radius fibers as a function of scale thickness (**w**) and temperature

>2.5 GPa (compression) and >300 MPa (tension) were calculated for thin and thick scales, respectively, at low temperatures. Scales formed at high temperature do not support significant self-pressures.

When comparing oxidation rates for bulk and fiber SiC, the difference in self-pressure between the two geometries is relevant. Both geometries have scale pressure. Calculations for the flat plate geometry are shown in figure 14. The difference in average pressure ($\mathbf{\Delta p_{av}}$) between a flat plate and a 6 μm radius fiber is shown in figure 15. Fibers with thick scales formed at low temperatures have the

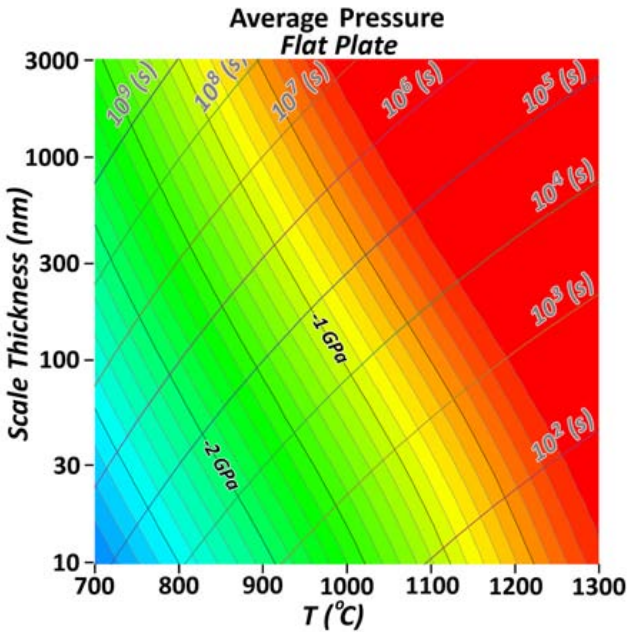

Fig. 14. Average SiO_2 scale self-pressure ($\mathbf{p_{av}}$) for a flat plate as a function of scale thickness (**w**) and temperature

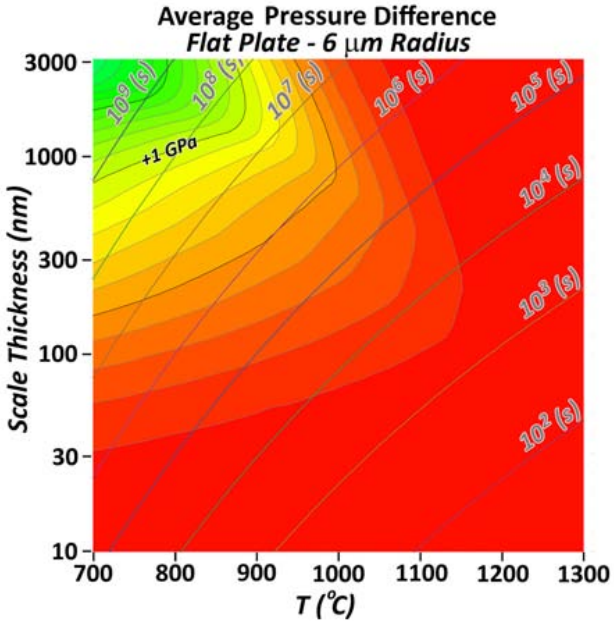

Fig. 15. The difference in average SiO_2 scale self-pressure ($\Delta\mathbf{p_{av}}$) between a flat-plate and a 6 μm radius fiber as a function of scale thickness (**w**) and temperature.

greatest Δp_{av}, and should therefore show the greatest enhancement relative to flat-plate oxidation kinetics.

For previously reported oxidation data for Hi-Nicalon™-S SiC fiber,[5-6] the highest Δp_{av} is ~500 MPa for ~1 μm thick SiO_2 scales formed at 1000°C (Fig. 15). By [52], the lower growth stresses (relative to flat plates) in fibers oxidized under these conditions would enhance **B** by ~8.5× in comparison to flat plates, increasing scale thickness by ~3×. This is at best only a partial explanation for the relatively high SiC oxidation rates for Hi-Nicalon™-S fiber. Most data, particularly that at 700° - 900°C and 1200° - 1300°C, has much lower Δp_{av} and the effects of growth stress would be insignificant.

It is interesting to note that the data of Gauthier et al. for stress dependence of the parabolic rate constant for Hi-Nicalon™ SiC fiber oxidation at 800°C is consistent with an 8× enhancement at ~500 MPa.[32] However, at higher stresses it is no longer consistent with [52].[32] At 1.276 GPa there is a measured enhancement of 19×, but [52] predicts enhancement by ~600×. We suggest that this is due to stress relaxation is the SiO_2 scale by [23], since shear stress is well above τ_c.

IV. Summary and Conclusions

A method to calculate the axial, hoop, and radial growth stresses in SiO_2 scales for the 2.2× volume expansion during SiC fiber oxidation was developed. Axial stresses are usually ignored, but for structural fibers they have the largest effect on strength. The method assumes oxidation volume expansion is three-dimensional (dilatational) and that the stresses resulting from constraint of that expansion are relaxed radially with an Eyring stress-dependent SiO_2 viscosity, although other appropriate viscosity models can be substituted. The method can be equally well applied to fibers of silicon or other materials. High compressive hoop and axial stresses of ~25 GPa are very quickly relaxed to much lower values at all temperatures. Stresses relax by radial expansion, which creates tensile hoop stress in the outer scale. Tensile hoop stress eventually drives axial stress to a tensile state by the Poisson effect. Tensile hoop and axial stress can reach values greater than 2 GPa for long times at 700° and 800°C. A continuum in stress response from flat plate geometry to small fiber radius geometry is demonstrated. The accuracy of the growth stress calculation method is limited by knowledge of accurate values for amorphous silica viscosity, which can be affected by incorporation of carbon or other impurities during SiC oxidation.

Tensile hoop and axial stresses reach steady-state values that can be described by analytical expressions. At steady-state, tensile stress relaxation rates are counterbalanced by hoop stress generation tied to the radial expansion of scale and the oxidation rate. At temperatures over 1200°C all growth stresses are rapidly relaxed by viscous flow to very low values. For Hi-Nicalon™-S SiC fibers, a 900°-1100°C oxidation temperature – 300 nm - 1 μm scale thickness window may exist where high tensile stresses at the scale surface are likely to develop. These may have negative effects on fiber mechanical properties. Even higher tensile stresses may develop for thicker scales at lower temperatures, but the times required to reach those thicknesses are very long.

Crystalline SiO_2 scales are assumed to have much higher viscosities than amorphous scales, and should therefore develop much higher tensile hoop and axial stresses than those scales. Unfortunately, lack of data on cristobalite and tridymite viscosity or creep rates, as well as diffusion rates, prohibits accurate quantitative prediction. However, qualitative predictions of high tensile stress in the outer scale and high shear stress near the SiC-SiO_2 interface are consistent with microstructure observations in crystalline silica scales.

Sample geometry may affect oxidation rates through the geometric effect on growth stresses. A Hi-Nicalon™-S SiC fiber and a flat plate of the same composition are calculated to have up to a ~500 MPa difference in average SiO_2 scale pressure from growth stress in thick scales formed at ~1000°C. This could increase scale thickness in the fiber by ~3× over that of the flat plate. However, the effect is smaller at higher and lower temperatures, and is currently only a partial explanation for higher fiber oxidation rates.

References

1. V. Presser and K. G. Nickel, Crit. Rev. Solid State Mater. Sci. **33**, 1-99 (2008).
2. I. Vickridge, J. Ganem, Y. Hoshino and I. Trimaille, J. Physics D: Applied Physics **40** (20), 6254 (2007).

3. G. Chollon, M. Czerniak, R. Pallier, X. Bourrat, R. Naslain, J. P. Pillot and R. Cannet, J. Mater. Sci. **32**, 893-911 (1997).
4. G. Chollon, R. Pallier, R. Naslain, F. Laanani, M. Monthioux and P. Olry, J. Mater. Sci. **32**, 327-347 (1997).
5. R. S. Hay, G. E. Fair, R. Bouffioux, E. Urban, J. Morrow, A. Hart and M. Wilson, Ceram. Eng. Sci. Proc. **32**, accepted (2011).
6. R. S. Hay, G. E. Fair, R. Bouffioux, E. Urban, J. Morrow, J. Somerson, A. Hart and M. Wilson, J. Am. Ceram. Soc. (2011 in press).
7. C. H. Hsueh and A. G. Evans, J. Appl. Phys. **54** (11), 6672-6686 (1983).
8. K. Garikipati and V. S. Rao, J. Computational Physics **174** (1), 138-170 (2001).
9. V. S. Rao and T. J. R. Hughes, Int. J. Numerical Methods in Engineering **47** (1-3), 341-358 (2000).
10. E. P. EerNisse, Appl. Phys. Lett. **35** (1), 8-10 (1979).
11. S. M. Hu, J. Appl. Phys. **70** (6), R53-R80 (1991).
12. V. Senez, D. Collard, B. Baccus, M. Brault and J. Lebailley, J. Appl. Phys. **76** (6), 3285-3295 (1994).
13. T. Uchida, M. Fujinaga, N. Kotani, S. Kawazu and H. Miyoshi, Jap. J. Appl. Phys. **35** (8), 4265-4273 (1996).
14. T. Uchida and K. Nishi, Jap. J. Appl. Phys. **40** (12), 6711-6719 (2001).
15. J. D. Evans, M. Vynnycky and S. P. Ferro, J. Eng. Math. **38**, 191-218 (2000).
16. M. Uematsu, H. Kageshima, K. Shiraishi, M. Nagase, S. Horiguchi and Y. Takahashi, Solid-State Electronics **48** (6), 1073-1078 (2004).
17. J. P. Peng, D. Chidambarrao and G. R. Srinivasan, COMPEL **10** (4), 341-353 (1993).
18. P. Causin, M. Restelli and R. Sacco, Computer Methods in Applied Mechanics and Engineering **193** (33-35), 3687-3710 (2004).
19. A. Pomp, S. Zelenka, N. Strecker and W. Fichtner, IEEE Trans. Elec. Dev. **47** (10), 1999-2007 (2000).
20. T. J. Delph, J. Appl. Phys. **83** (2), 786-792 (1998).
21. D.-B. Kao, J. P. McVittie, W. D. Nix and K. C. Saraswat, IEEE Trans. Electron. Dev. **35** (1), 25-37 (1988).
22. C. S. Rafferty, L. Borucki and R. W. Dutton, Appl. Phys. Lett. **54** (16), 1516-1518 (1989).
23. N. F. Mott, S. Rigo, F. Rochet and A. M. Stoneham, Philos. Mag. B **60** (2), 189-212 (1989).
24. M. Navi and S. T. Dunham, J. Electrochem. Soc. **144** (1), 367-371 (1997).
25. P. Sutardja and W. G. Oldham, Electron Devices, IEEE Transactions on **36** (11), 2415-2421 (1989).
26. R. H. Doremus, Thin Solid Films **122** (3), 191-196 (1984).
27. K. Imai and K. Yamabe, J. Appl. Phys. **83** (7), 3849-3855 (1998).
28. R. B. Marcus and T. T. Sheng, J. Electrochem. Soc. **129** (6), 1278-1282 (1982).
29. A. Mihalyi, R. J. Jaccodine and T. J. Delph, Appl. Phys. Lett. **74** (14), 1981-1983 (1999).
30. J.-Y. Yen and J.-G. Hwu, Appl. Phys. Lett. **76** (14), 1834-1835 (2000).
31. J.-Y. Yen and J.-G. Hwu, J. Appl. Phys. **89** (5), 3027-3032 (2001).
32. W. Gauthier, F. Pailler, J. Lamon and R. Pailler, J. Am. Ceram. Soc. **92** (9), 2067-2073 (2009).
33. E. Oh, J. Walton, D. Lagoudas and J. Slattery, Acta Mechanica **181** (3), 231-255 (2006).
34. C. S. Rafferty and R. W. Dutton, Appl. Phys. Lett. **54** (18), 1815-1817 (1989).
35. H. Eyring, J. Chem. Phys. **4**, 283-291 (1936).
36. A. A. Wereszczak, M. Karakus, K. C. Liu, B. A. Pint, R. E. Moore and T. P. Kirkland, ORNL/TM-13757, 1-61 (1999).
37. A. A. Wereszczak, K. Breder, M. K. Ferber, T. P. Kirkland, E. A. Payzant, C. J. Rawn, E. Krug, C. L. Larocco, R. A. Pietras and M. Karakus, J. Mater. Sci. **37** (19), 4235-4245 (2002).
38. M. K. Ferber, A. A. Weresczak and J. G. Hemrick, Final Technical Report ORNL/TM-2005/134, 1-67 (2006).

39. L. O. Wilson and R. B. Marcus, J. Electrochem. Soc. **134** (2), 481-490 (1987).
40. B. E. Deal and A. S. Grove, J. Appl. Phys. **36** (12), 3770-3778 (1965).
41. Y. C. Tsui and T. W. Clyne, Thin Solid Films **306**, 34-51 (1997).
42. P. P. Donnadieu, O. Jaoul and M. Kleman, Philos. Mag. A **52** (1), 5-17 (1985).
43. R. H. Doremus, J. Appl. Phys. **92** (12), 7619-7629 (2002).
44. G. Hetherington, K. H. Jack and J. C. Kennedy, Phys. Chem. Glasses **5** (5), 130-136 (1964).
45. T. Rouxel, G.-D. Soraru and J. Vicens, J. Am. Ceram. Soc. **84** (5), 1052-1058 (2001).
46. J. H. Li and D. R. Uhlmann, J. Non. Cryst. Sol. **3** (1), 127-147 (1970).
47. L. E. Malvern, *Introduction to the Mechanics of a Continuous Medium*, 1st ed. (Prentice-Hall, 1969).
48. A. Polian and et al., Europhys. Lett. **57** (3), 375 (2002).
49. T. Narushima, M. Kato, S. Murase, C. Ouchi and Y. Iguchi, J. Am. Ceram. Soc. **85** (8), 2049-2055 (2002).
50. M. I. Chaudhry, J. Mater. Res. **4** (2), 404-407 (1989).
51. C. E. Ramberg, G. Cruciani, K. E. Spear, R. E. Tressler and C. F. Ramberg, J. Am. Ceram. Soc. **79** (11), 2897-2911 (1996).
52. U. J. T. Ogbuji and E. J. Opila, J. Electrochem. Soc. **142**, 925-930 (1995).
53. G. M. Renlund, S. Prochazka and R. H. Doremus, J. Mater. Res. **6** (12), 2723-2734 (1991).
54. T. Rouxel, G. Massouras and G.-D. Soraru, J. Sol-Gel Sci. Tech. **14**, 87-94 (1999).
55. V. Presser, A. Loges, Y. Hemberger and K. G. Nickel, J. Am. Ceram. Soc. **92** (3), 724-731 (2009).
56. V. Presser, A. Loges, Y. Hemberger and K. G. Nickel, J. Am. Ceram. Soc. **92** (8), 1796-1805 (2009).
57. H. J. Frost and M. F. Ashby, *Deformation Mechanism Maps*. (Pergamon Press, 1982).